DOI: 10.1109/TASC.2024.3350606
FERMILAB-PUB-24-0114-TD (accepted)

Quench Behavior of 18-mm-period, 1.1-m-long Nb_3Sn Undulator Magnets

I. Kesgin, S. MacDonald, M. Kasa, J. Fuerst, Y. Ivanyushenkov, E. Barzi, Senior Member, IEEE, D. Turrioni, A. V. Zlobin and E. Gluskin

Abstract—A novel Nb_3Sn-based superconducting undulator (SCU) was developed and integrated into the Advanced Photon Source (APS) at Argonne National Laboratory. The SCU achieved user operation within an accelerator environment. Compared to its Nb-Ti counterpart, the Nb_3Sn SCU operates at substantially higher currents. Thus, a detailed experimental evaluation of the SCU magnets' performance was necessary under both "wet" and indirectly cooled conditions to ensure its reliability during operation. Our study indicated that the cooling method has a noticeable influence on the magnet's behavior. Specifically, energy dissipation in the magnets during quenches was observed to be greater under indirect cooling than with "wet" cooling. This investigation provided insights into the safe operational limits. Guided by these insights the more challenging high-current tests were successfully carried out at the end of the user phase. The SCU achieved the design undulator field of 1.17T at 820A and 4.2K, with a magnetic gap of 9.5 mm and a period of 18 mm. Actual performance exceeded the specifications, reaching 850A.

Index Terms—Nb_3Sn, superconducting undulator, SCU, stability, magnet design, quench energy, dissipations, quench back, losses

I. Introduction

THE Advanced Photon Source (APS) at Argonne National Laboratory has marked a milestone by successfully deploying the Nb_3Sn superconducting undulator (SCU) in its storage ring. This innovative device was in use throughout the last APS run prior to the storage ring upgrade. To the best of our knowledge, this stands as the sole Nb_3Sn accelerator magnet functioning in a real accelerator context.

The project primarily aimed at developing technology for fabricating Nb_3Sn SCUs, demonstrating an increase in the undulator field compared to NbTi SCUs. This paper will particularly concentrate on the quench analysis of the Nb_3Sn SCU magnets, which played a crucial role in ensuring that they consistently delivered the expected performance and functioned reliably without issues during the user run.

Manuscript received on September 22, 2023. This research used resources of the Advanced Photon Source, in part U. S. Department of Energy (DOE) Office of Science User Facility at Argonne National Laboratory, and in part by the U.S. DOE Office of Science-Basic Energy Sciences, under Grant DE-AC02-06CH11357. (Corresponding author: Ibrahim Kesgin)

I. Kesgin, S. MacDonald, M. Kasa, J. Fuerst, Y. Ivanyushenkov, and E. Gluskin are with Advanced Photon Source, Argonne National Laboratory, Lemont, IL 60439 USA (e-mail: ikesgin@anl.gov).

D. Turrioni, E. Barzi, and A. V. Zlobin are with Fermilab, Batavia, IL 60510 USA.

Color versions of one or more figures in this article are available at ...Digital Object Identifier

TABLE I
Nb_3Sn SCU Specifications

Parameters	Value
Design max. undulator field	1.17 T
Magnetic Length	1.1 m
Design maximum current	820 A (~70% of I_c)
Magnetic gap	9.5 mm
Number of turns in a coil pack	46
Number of periods	59.5
Groove width and depth	5.35 mm and 5 mm
Period length	18 mm
Superconductor and non-Cu fraction	RRP 144/169 and ~48%
Wire diameter and insulation thickness	0.6 mm and 65 μm

The high operating current density of the Nb_3Sn SCU requires an advanced quench detection and protection system (QDPS). An active protection method was conceived in collaboration with Lawrence Berkeley National Laboratory [1].

Simulating quench events is challenging, given the difficulty in pinpointing accurate material properties. The rapid current decay time constant of SCU magnets sets them apart from many other SC magnet variants. The fast decay with the resulting dB/dt leads to large dynamic losses, which not only facilitate quench distribution but also complicate simulations. This process generally is called "quench-back (QB) effect". While simulations provide guidance for the quench protection system, the bedrock of our safety strategy is empirical quench analyses. The following sections provide some details on the magnet fabrication and an in-depth examination of the quench behaviors of the 1.1-m-long Nb_3Sn SCU magnets under two different cooling configurations.

II. Fabrication of 1.1-m-long Nb_3Sn SCU Magnet

Table I presents a summary of the Nb_3Sn SCU parameters. Further insights on the fabrication steps can be found in [2-7]. The design is based on the APS's previous SCU versions [2, 8, 9]. The magnets were wound in ANL and transported to Fermilab to be heat treated (HT), then transported back to ANL for the following fabrication and characterizations steps. The HT cycle was optimized through several small prototypes [5, 7, 10] to suppress flux jump instabilities.

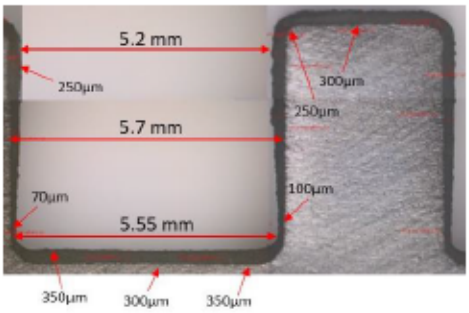

Fig 1. Optical microscope image of the Al_2O_3 plasma-sprayed groove, displaying varying dimensions across different regions. Thickness measurements range from as thin as 70 μm to as thick as 350 μm.

A. Coil-to-Ground Insulation – Al_2O_3 Plasma Spraying

During quench events, high voltages arise, and a coil-to-ground insulation is integral to prevent dielectric breakdowns. However, the HT process considerably restricts the selection of materials.

The Al_2O_3 plasma spraying process, a frequently used coating technique in aerospace applications, was chosen to coat the magnet low carbon steel (LCS) cores. This technique generates a plasma zone, through which Al_2O_3 powders are propelled, adhering to the targeted surface. Due to the inherent randomness of this method, the resulting coatings often exhibit non-uniform thickness. Fig. 1 presents a cross-section of the coated LCS core, illustrating the variations in thickness. These differences can be substantial, ranging from 70 μm to 350 μm. Visual inspections of the coating further revealed significant contrasts. It became challenging to ascertain whether darker areas were uncoated or merely had an extremely thin layer, particularly since the Al_2O_3 layer can appear transparent. Despite considerable efforts to optimize and achieve a more uniform result, the final coatings remained less consistent than desired.

Such inconsistency in the coating thickness emerged as a primary contributor to the magnet failure. For quality control purposes, we consistently monitored the coil-to-ground resistance. After the winding, this resistance was very high, basically infinite. However, post-HT, the resistance readings were notably lower, i.e., in the kΩ range. We noticed that the resistance gradually increases as the magnets cooling down and decreases upon warming up, a characteristic reminiscent of semiconductor behavior. Residues from the organic binder material in the braided insulation are the most likely reason for this behavior. We are currently investigating a more efficient removal method for these residues during the HT process.

III. Results and Discussions

A. Individual Magnet Training

Before evaluating the magnets in the undulator setup, each magnet was individually placed inside a vertical cryostat and cooled to 190 K using liquid nitrogen in the outer jacket. The assembly was then further cooled to liquid helium (LHe) temperature by transferring LHe to the inner reservoir.

Magnet training at LHe temperature is illustrated in Fig. 2. Both magnets show similar training behavior. The peak training currents for individual magnets reached to 936A for M1 (Magnet 1) and 905A for M2 (Magnet 2) in the first cool down. The magnets underwent subsequent cooling cycles and achieved their maximum design current without needing additional training, reaching 960A for M1 and 920A for M2. The same figure also presents the short sample limits (SSLs) for the two magnets calculated based on witness sample data, depicting the potential for further performance enhancement for both magnets. The SSL for M1 (1160A) is smaller than that for M2 (1204A). The measured residual resistivity ratios (RRRs) from the short samples also differ, being 82 for M1 and 117 for M2.

B. Magnet Cooling Schemes – LHe Bath & Indirect Cooling

The Nb_3Sn SCU magnets were tested in two distinct configurations: in a vertical LHe bath cryostat (directly cooled by a liquid helium bath), and in an indirectly cooled horizontal cryostat. In the indirect cooling method, a specifically designed central cooling channel, drilled into the magnet, was filled with LHe, facilitating the cooling of the magnet windings from within. The effect of cooling scheme is discussed below.

C. Magnet Voltage Analysis

After individual quench training, the magnets were assembled into an undulator configuration and further tested. The assembly was charged to 800A without requiring additional training. During quench measurements, artificial quenches were induced, the quench detection system was manually triggered, and the current-voltage dynamics captured. This approach facilitated a more refined comparison between the magnets. The behavior of the undulator magnets was not uniform as it was marked by voltage deviations between M1 and M2 in Fig 3. This non-uniformity became evident when dynamic losses caused the SC volume to transition into a non- SC state, leading to an increase in internal resistance. Most of the stored energy is dissipated into the magnet with the lower I_c and lower RRR.

The magnet behaviors depend on the cooling schemes. Indirect cooling exacerbated the non-uniform behavior, as it accelerated quench propagation. As a result, voltage deviations between the magnets became more evident, an effect illustrated in

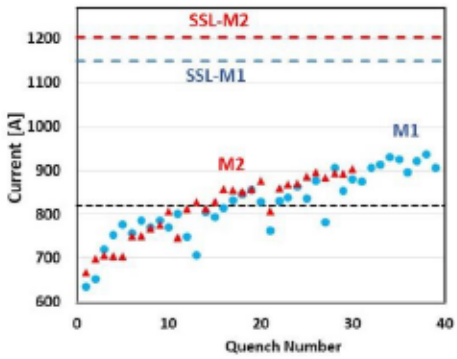

Fig 2. Training profiles for M1 and M2 with comparison of their respective short sample limits. Individual magnets were trained up to 905 for M2 and 936A for M1, respectively in the first cool down.

Fig. 3. The QB effect in the indirectly cooled setup started about 2 ms earlier. This earlier onset of the QB effect causes greater energy dissipation in the magnets and less extraction by the dump resistors, as will be explained later in this section. The figure also depicts the corresponding current decays. In an indirectly cooled configuration, current decays more swiftly.

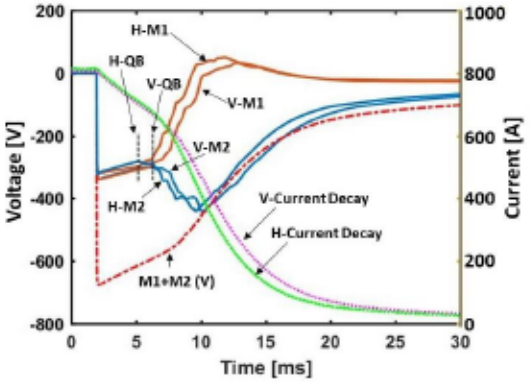

Fig. 3. Voltage profiles (left) and current decays (right) observed during a quench in the two different cooling schemes. Points where the quench-back (QB) effect starts are also displayed. "V" represents results for the vertical tests (LHe bath), while "H" denotes horizontal tests (indirectly cooled).

Combined with the uneven thickness of the ground insulation, these observations informed the decision to set a maximum operational current limit of 700A (1.04T) during standard runs, keeping higher current tests for the end of the user run. After three months of stable operation, the magnets were tested beyond the current threshold up to 850A, confirming their optimal performance. Reaching this current level necessitated only two quenches. Additional intentional quenches were introduced from these high current levels, which did not compromise the e-beam stability and did not introduce any beam loss. Magnets stably operated at this high current level with the regular operational beam current of 100 mA.

D. Hot Spot Temperature

During a quench, a localized region, termed the "hot spot" (HS), experienced a rapid temperature rise. The temperature of this region can be computed adiabatically by integrating I^2 over time using temperature-dependent material properties. The calculated HS temperatures using this method are provided in

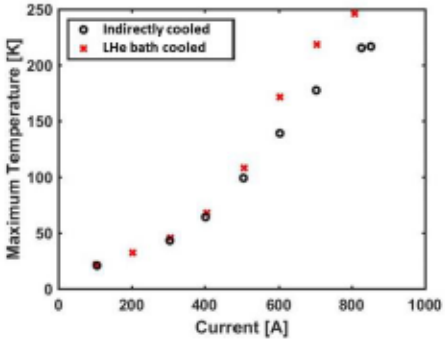

Fig. 4. Calculated hot spot temperature versus current for the two different cooling schemes. Indirect cooling causes faster current decay and lowers the temperatures.

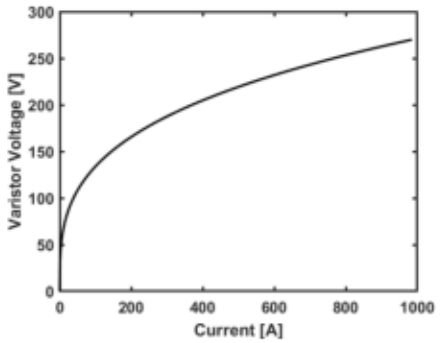

Fig. 5. Varistor voltage at different currents. Resistance increase is rapid up to 600A, and then it slows down.

Fig. 4. These computations account for a 2-ms detection time. The target temperature is to keep it below the safe limit of 300 K.

Similar to the observed voltage profiles, the calculated HS temperatures exhibit variances contingent upon the employed cooling methodologies. These discrepancies are particularly emphasized at elevated currents, i.e., larger than 600A, where QB effects are pronounced. In the case of indirectly cooled magnets, the HS temperatures tend to be lower due to earlier start of the QB and the faster quench propagation.

E. Energy Dissipations – Magnets and Resistor & Varistor

During the electromagnetic tests of the magnets, the current-dependent inductance, $L(I)$, was measured. The energy deposited on the resistor/varistor can be determined by integrating the product of $V(t)$ and $I(t)$ with respect to time. The stored energy can be calculated from the formula $L(I)\, I(t)^2/2$.

As seen in Fig. 7, approximately 40% of the total stored energy is extracted through the resistor/varistor circuit at an 800A level. The dump resistor has a value of 0.56 Ohms. The behavior of the varistor (I vs. V curve) is current dependent and is shown in Fig. 5. We adjusted the varistor value to increase resistance rapidly up to an intermediate current of 700A, after which it increases more slowly. This is because the dynamic losses contribute to the magnet resistance at higher currents, and the overall system possesses a relatively higher resistance at current levels greater than 700A. However, this effect is less pronounced at intermediate current levels (500-700A), necessitating higher resistance values. Using a linear resistor would cause the voltage to rise significantly at higher currents, potentially leading to insulation failure. The varistor is integrated to mitigate this. However, the calculated varistor values were insufficient, so we had to pair it with a linear resistor in series.

F. Pressure Analysis in the LHe Reservoir

For a system containing a saturated liquid-vapor mixture, the total energy (E) can be determined by considering the energy of both the liquid and vapor phases. The volume is 100 liters, which remains constant and encompasses both liquid, 23.5 liters, and vapor at 755 Torr.

The quality x_1, which represents the mass ratio of the vapor given by $m_{vapor} / (m_{vapor} + m_{liquid})$, can be used to find the initial specific internal energy of the mixture:

$$u_1 = u_{f1}(1 - x_1) + u_{g1}x_1,$$

where u_f is the specific internal energy of the saturated liquid and u_g is the specific internal energy of the saturated vapor

Similarly, using the quality x_2 for the final state, the final specific internal energy can be determined as:

$$u_2 = u_{f2}(1 - x_2) + u_{g2}x_2.$$

For a system with mass m, the energy change ΔE is:

$$\Delta E = m(u_2 - u_1).$$

This formula assumes that the only form of energy being considered is internal energy, neglecting other forms.

The pressure increase inside the LHe reservoir during a quench is recorded using a pressure transducer, as shown in Fig. 6 (right axis), alongside the SCU's operating current on the left axis with a maximum of 850A just before the initiation of the intentional quench. The peak observed pressure reaches 950 Torr right after the quench. At this point, the liquid is in a subcooled state, and the vapor is superheated. The pressure gradually recedes to its baseline within an hour, facilitated by the recondensation of the vapor due to cooling effects provided by the cryocoolers.

The HEPAK Excel add-in was used for calculating the thermophysical properties of helium. Given the observed pressure rise during a quench, the energy required to elevate the pressure to this level can be found. In Fig. 7, bottom, the computed energy values called LHe Dissipation (represented by red circles) are compared with results from the values computed from the electrical circuit analysis (illustrated by a dashed dark blue curves). Both sets of calculations are in perfect agreement and represent the energy dissipated into the magnets. The same analysis is not possible in the LHe bath cooling case since the He vapor is not collected.

In Fig. 7, the energy dissipation into the resistor/varistor (called extracted by Res.+Var.) and the magnets are also depicted with the LHe bath cooling case at the top and the indirectly cooled case at the bottom. As anticipated, the total stored energy is consistent in both situations as inductance does not change with different cooling type. However, energy dissipations into the magnets and resistor/varistor show slight differences at high current levels. Notably, the resistor and varistor in the LHe bath cooled configuration extracts more energy, 46% vs 39% in the indirectly cooled case at operating currents around 800A.

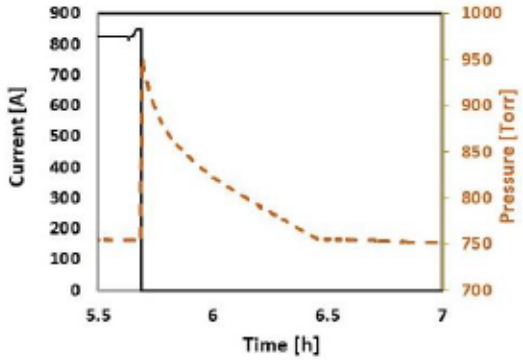

Fig 6. The current (left) is at 850A just prior to the onset of the quench. The pressure (right) swiftly rises to 950 Torr and then gradually returns to the regular operating pressure within an hour.

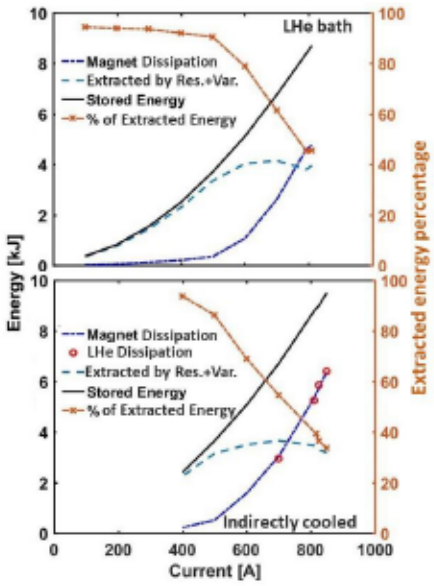

Fig 7. Energy dissipations during quenches from various current levels. The top plot displays results for LHe bath tests (wet), while the bottom plot represents the indirectly cooled configuration. In both scenarios, the majority of the stored energy is extracted via resistor/varistor at lower current levels while reducing gradually as current increases.

IV. Conclusion

A novel Nb_3Sn SCU with a magnetic gap of 9.5 mm and a period of 18 mm was fabricated, installed and operated at the APS. Experimental quench analysis of the Nb_3Sn SCU magnets was one of the key factors that contributed to the successful operation of the Nb_3Sn SCU. The magnet quench behavior, observed during testing, exhibited slight variations based on the chosen cooling scheme. Quench energy estimates from voltage-current analysis were consistent with values from pressure analysis in the LHe tank. It was identified that one magnet absorbs higher energy during a quench, a condition that was further exacerbated by indirect cooling. Non-homogeneous magnet behavior, combined with a non-consistent coil-to-ground insulation thickness, poses a risk of dielectric breakdown, and a decision was made to postpone the high-current testing to the end of the user run. Then, these tests were concluded successfully, and the device surpassed the anticipated design performance.

Acknowledgments

The authors would like to thank members of the ASD, AES and XSD teams of the APS for technical and design support; the Fermilab team for the HT studies for optimizing the stability of the Nb_3Sn wire, HTs of the magnets, and measurements of the short sample limits; and the LBNL team for quench simulations, design, and fabrication of the QDPS.

REFERENCES

[1] K. Edwards, L. Brouwer, I. Kesgin, D. Arbelaez, R. Teyber, and S. Prestemon, "Quench Behavior of Nb_3Sn Superconducting Undulator Magnets," *to be submitted to*.

[2] Y. Ivanyushenkov *et al.*, "Status of the Development of Superconducting Undulators at the Advanced Photon Source," *Synchrotron Radiat. News,* vol. 31, no. 3, pp. 29-34, May 2018, doi: 10.1080/08940886.2018.1460172.

[3] I. Kesgin *et al.*, "Fabrication and Testing of 18-mm-Period, 0.5-m-Long Nb_3Sn Superconducting Undulator," *IEEE Trans. Appl. Supercond.,* vol. 31, no. 5, Feb. 2021, Art. no. 4100205, doi: 10.1109/TASC.2021.3057846.

[4] I. Kesgin *et al.*, "Fabrication and Testing of 10-Pole Short-Period Nb_3Sn Superconducting Undulator Magnets," *IEEE Trans. Appl. Supercond.,* vol. 30, no. 4, Jun. 2020, Art. no. 4100605, doi: 10.1109/TASC.2020.2964193.

[5] I. Kesgin *et al.*, "Development of Short-Period Nb_3Sn Superconducting Planar Undulators," *IEEE Trans. Appl. Supercond.,* vol. 29, no. 5, Feb. 2019, Art. no. 4100504, doi: 10.1109/TASC.2019.2897645.

[6] A. V. Zlobin *et al.*, "Advantages and Challenges of Nb_3Sn Superconducting Undulators," in *9th Int'l. Part. Accel. Conf. (IPAC18)*, Vancouver, BC, Canada, 2018, pp. 2734-2727, doi:10.18429/JACoW-IPAC2018-WEPML025.

[7] E. Barzi *et al.*, "Heat Treatment Studies of Nb_3Sn Wires for Superconducting Planar Undulators," *IEEE Trans. Appl. Supercond.,* vol. 30, no. 4, Mar. 2020, Art. no. 6001005 doi: 10.1109/TASC.2020.2974706.

[8] Y. Ivanyushenkov *et al.*, "Development and operating experience of a 1.1-m-long superconducting undulator at the Advanced Photon Source," *Phys. Rev. Accel. Beams,* vol. 20, no. 10, Oct. 2017, Art. no. 100701, doi: 10.1103/PhysRevAccelBeams.20.100701.

[9] M. Kasa *et al.*, "Development and operating experience of a 1.2-m long helical superconducting undulator at the Argonne Advanced Photon Source," *Phys. Rev. Accel. Beams,* vol. 23, no. 5, May 2020, Art. no. 050701, doi: 10.1103/PhysRevAccelBeams.23.050701.

[10] I. Kesgin *et al.*, "Design, Construction, and Testing of 0.5-m, 18-mm Period Nb_3Sn Superconducting Undulator Magnets," *IEEE Trans. Appl. Supercond.,* vol. 32, no. 6, Sep. 2022, Art. no. 4100605, doi: 10.1109/TASC.2022.3152712.